An Organic-Inorganic Hybrid Exhibiting Electrical Conduction and Single-Ion-Magnetism

Yongbing Shen, *,[†] Goulven Cosquer, *,[†] Hiroshi Ito,[ξ] David Chukwuma Izuogu,[‡,§] Alex J.W. Thom,[‡] Toshiaki Ina,[ǁ] Tomoya Uruga,[ǁ] Takefumi Yoshida,[⊥] Shinya Takaishi,[†] Brian K. Breedlove,[†] Zhao-Yang Li,[⊗] and Masahiro Yamashita*,[⊗,¶,†]

[†] Department of Chemistry, Graduate School of Science, Tohoku University, 980-8578 Sendai, Japan

[ξ] Department of Applied Physics, Nagoya University, Chikusa-ku, Nagoya 464-603, Japan

[‡] Department of Chemistry, University of Cambridge, Lensfield Road, Cambridge, CB2 1EW United Kingdom

[§] Department of Pure and Industrial Chemistry, University of Nigeria, Nsukka, 410001, Enugu State, Nigeria

[ǁ] Research & Utilization Division, Japan Synchrotron Radiation Research Institute, 1-1-1 Kouto, Sayo, Sayou-gun, Hyogo 679-5198, Japan

[⊥] Electronic Functional Macromolecules Group, National Institute for Materials Science (NIMS), Tsukuba 305-0044, Japan

[⊗] School of Materials Science and Engineering, Nankai University, Tianjin 300350, China

[¶] WPI-Advanced Institute for Materials Research (AIMR), Tohoku University, 2-1-1 Katahira, Aoba-ku, Sendai 980-8577, Japan

ABSTRACT

The first three–dimensional (3D) conductive single-ion magnet (SIM), $(TTF)_2[Co(pdms)_2]$ (TTF = tetrathiafulvalene and H_2pdms = 1,2-bis(methanesulfonamido)benzene), was electrochemically synthesized and investigated structurally, physically and theoretically. The quite close oxidation potential between neutral TTF and the coordination precursor, $(HNEt_3)_2[M(pdms)_2]$ (M = Co, Zn) causes multiple charge transfers (CTs) between SIM donor $[M(pdms)_2]^{n-}$ and the $TTF^{\bullet+}$ acceptor as well as an intra-donor CT from the pdms ligand to Co ion upon electrocrystallization. Usually TTF works as a donor, whereas in our system, TTF works as both a donor and an accepter due to the close oxidation potentials. Furthermore, the $[M(pdms)_2]^{n-}$ donor and $TTF^{\bullet+}$ acceptor are not segregated but strongly interact with each other, contrary to reported layered donor-acceptor electrical conductors. The strong intermolecular and intramolecular interactions, combined with the CT, cause relatively

high electrical conductivity to very low temperature. Furthermore, SIM behaviour with slow magnetic relaxation and opening of hysteresis loops were observed. $(TTF)_2[Co(pdms)_2]$ (**2-Co)** is an excellent building block for preparing new conductive SIM.

INTRODUCTION

Delocalized charge carrier transport in crystalline solids requires carrier pathway made of specific crystalline arrangement such as segregated stacks of partially-oxidized molecules with good orbital overlaps.[1] The π−conjugated planar molecules, such as tetrathiafulvalene (TTF) and tetracyano-quinodimethane (TCNQ), favors to form π–π stacking motifs to maximize the frontier orbital overlap, therefore, they are widely used to design the electronically active materials,[2] such as donor-acceptor CT salts,[3] conducting metal-organic frameworks (MOFs), etc.[4] However, in the case of bifunctional materials aiming to couple between magnetism and conduction, especially the layered magnetic conductors, such as $[BEDT\text{-}TTF]_3[MnCr(C_2O_4)_3]$,[1a] $[BEDO\text{-}TTF]_6K_2[BW_{12}O_{40}]\cdot 11H_2O$,[5] such segregated stack structure often prevents the localized spins in the magnetic sublattice from interacting with the conducting sublattice made of π-conjugated molecules.[1a, 6]

Single-ion magnets are molecular compounds with a significant energy barrier for the spin reversal behaviour at the molecular level[7] and can be used for information storage,[8] spin-valves or quantum computing, etc.[9] The magnetic bistabililty of SIM is characterized by the presence of an energy barrier (Δ) between two spin-states.[10] Δ is governed by ground state spins (S_T) and magnetic uniaxial anisotropy, described by large negative zero-field splitting parameter along the easy-axis (D) and a small zero-field splitting parameter in the easy-plane (E) in the following anisotropic Hamiltonian term: $H = DS_{Tz}^2 + E(S_{Tx}^2 - S_{Ty}^2)$. $\Delta = |D|S_T^2$ for integer values of S_T and $\Delta = |D|(S_T^2 - 1/4)$ for half-integer values of S_T.

Since the discovery of SIM , researchers have perceived several potential applications, which have become key research topics in the area of molecular quantum spintronics.[11] Combining SIM behavior and electrical conductivity may bring about the giant-magnetoresistance and be advantageous for the next generation of high-density information storage media.[12] Molecular spin qubits,[13] and supramolecular spin valves[14] have been realized via ingenious engineering design. At the same time, although hybrids of SIM and electrical conductors with layered structures have been reported,[15] synergy between magnetic lattice and conducting lattice is still challenging for materials chemists. The two phenomena in these reported materials tend to originate from two different sublattices in different temperature regions, further hinder the electronical interaction. Ligands have been demonstrated to be crucial for inducing the electronical interaction in such bifunctional materials. Herein, we introduce a strategy to incorporate strong interactions between π−conjugated redox-active SIM and conducting sublattice with the use of TTF molecule to afford the conductive SIM $(TTF)_2[Co(pdms)_2]$ (**2-Co**) and the isostructural $(TTF)_2[Zn(pdms)_2]$ (**2-Zn**). Introduction of redox-activity on ligand is the first time to prepare conducting SIM material. The H_2pdms ligand is a σ and

π electron donor[16] with quite similar redox activity to TTF upon formation of metal complex, causing the frontier orbitals of the ligand and TTF to overlap, yielding electrical conductivity down to 2 K. Moreover, the tetrahedrally coordination geometry of [M(pdms)$_2$], combined with TTF, leads to an unusual 3D mixed stacking framework compared to those reported 2D layered conductive SIM compounds. SIM behaviors are still observed in **2-Co** even the reduction of Co(II) ions occurred during the CT process.

Experimental methods

H_2pdms, $CoCl_2$, $ZnCl_2$, TTF and organic solvents were commercially purchased and used without further purification. The precursors $(HNEt_3)_2$[Co(pdms)$_2$] (**1-Co)** and $(HNEt_3)_2$[Zn(pdms)$_2$] **1-Zn** were synthesised following a reported procedure.[16]

Preparation of (TTF)$_2$[M(pdms)$_2$]: A solution of 20 mg TTF and 80 mg of **1-Co** (or **1-Zn**) in 15 mL of dry acetonitrile was filtered, and the resulting clear solution was placed in an electrocrystallization cell under a N_2 gas atmosphere. A 0.5 μA dc current was then applied. Small black needle-shaped crystals of size typically 50 μm × 5 μm × 5 μm grew on the anode over 10 days, and then they were collected, washed with a small amount of ethanol and dried in air. Yield: 20 mg (36% based on TTF). Elemental analysis: $C_{28}H_{28}N_4O_8S_{12}Co$ Calcd.: C, 33.89; H, 2.84; N, 5.65. Found: C, 34.42; H, 3.41; N, 6.14. $C_{28}H_{28}N_4O_8S_{12}Zn$: Calcd.: C, 33.67; H, 2.83; N, 5.61. Found: C, 34.27; H, 2.97; N, 5.94. For 2-$Co_{0.1}Zn_{0.9}$, the same procedure was used except 10 mg of **1-Co** and 90 mg of **1-Zn** was used.

Physical characterisation: Single-crystal crystallographic data were collected at 100 K on a Rigaku Mercury CCD Diffractometer with synchrotron radiation (λ = 0.68890 Å) produced by KEK PF-AR NW2A beamline source. Data processing was performed using the CrysAlis(Pro) and the Crystal Clear crystallographic software package.[17] The structures were solved by using direct methods included in SIR-92[18] and refinement was carried out using SHELXL-2013.[19] The non-H atoms were refined anisotropically using weighted full-matrix least squares, and H atoms attached to the C atoms were positioned using idealized geometries and refined using a riding model.

X-ray absorption near edge structure (XANES) spectra were obtained in the BL01B1 beamline of JASRI/Spring-8 synchrotron, Japan, and data analysis were done using the Athena package.[20] Elemental analyses were performed at the Research and Analytical Centre for Giant Molecules, Tohoku University. The phase purity was confirmed by using powder X-ray diffraction on a Bruker D2 Phaser (Figure S1). Cyclic voltammetry was performed using an ALS/HCH Model 620D electrochemical analyzer. A glassy carbon (3 mm diameter) electrode was used as the working electrode, a Pt wire was used as the counter electrode, and an Ag wire was used as the reference electrode. The supporting electrolyte was 0.1 M tetrabutylammonium hexafluorophosphate ($TBAPF_6$) in dry acetonitrile.

UV-Vis spectra were acquired in the solid-state as KBr pellets on a Shimadzu UV-3100pc. Magnetic susceptibility measurements were conducted on a polycrystalline sample using a Quantum Design SQUID magnetometer MPMS-7L. The diamagnetic corrections were estimated from Pascal's constants.[21] Ac measurements were performed in a frequency range of 0.1–1000 Hz on a Quantum Design SQUID magnetometer MPMS-7L and 10–10000 Hz on a Quantum Design PPMS 6000. In both cases, an ac field amplitude of 3 Oe was applied, and the data from both machines were combined before fitting. Magnetoresistances and temperature dependences of the electrical conductivities were measured on a Quantum Design PPMS 6000 by using a four-probe method with samples compressed as pellets at a pressure of 39.2 MPa. Measuring current and magnetic field direction on the sample is illustrated in Figure S2.

Calculation methods: The crystal structure obtained from single crystal X-ray diffraction was used without geometry optimization to avoid charge transfer energy variance due to the angular dependence of charge transfer,[22] and cobalt and zinc ions were initialized in +2 oxidation states. The energy decomposition analysis (EDA) was carried out by employing the second-generation absolutely localized molecular orbital method (ALMO-EDA2),[23] as implemented in Q-Chem software package.[24] The molecular calculations for the EDA (unrestricted with total spin multiplicity of 6) was carried out using the DEF2-SVP[25] basis set for all atoms at the B3LYP level[26] with revPBE and PBE for dispersive exchanges and correlations, respectively.[27] The basis set superposition error (BSSE)[28] was corrected by employing a counterpoise correction.[29] For the LOBA,[30] the Pipek-Mezey (PM)[31] localization procedure and Lowdin population analysis were employed at the same level of theory and basis set as in EDA.[32] The ORCA software package[33] was used for the time-dependent density functional theory (TD-FT) calculations with the same level of theory and basis set as used for the Q-Chem calculations. Electronic band structures and density of states (DOS) were calculated using the pseudopotential plane-wave method, as implemented in the quantum espresso package (version 6.3),[34] following the pathway determined by using Seek-path (Figure S3).[35] The ultrasoft pseudopotential method to describe the interaction between ions and valence electrons was utilised (pbe-n-rrkjus_psl.1.0.0.UPF). The PBE functional within the generalised gradient approximation (GGA) was applied for the exchange-correlation interactions between the valence electrons. As major computational parameters, the plane-wave cut off energies were set as 46 Ry for the wave function and 460 Ry for the electron density, and the Monkhorst−Pack special k points were set as (5×5×5) for all of the supercell models. The self-consistent convergence threshold for the total energy was 10^{-6} Ry. The Fermi−Dirac function with a Gaussian spreading factor of 0.01 Ry was applied to the Brillouin zone integration.

Results

Crystal structure. Since **2-Co** and **2-Zn** are isostructural, only **2-Co** will be described in detail. The $TTF^{\bullet+}$ and $Co(pdms)_2$ units electrocrystallized in the *C2/c* space group (Table S1) with one $TTF^{\bullet+}$

and 0.5 $Co(pdms)_2$ molecules per asymmetric unit (Figure S4). The Co ion is coordinated to two pdms ligands through the N atoms in a tetrahedral geometry. The Co-N1 and Co-N2 bond lengths were determined to be 1.958 and 2.038 Å, respectively, and the dihedral angle between the two pdms ligands was determined to be 81.4°. The $TTF^{\bullet+}$ molecule is almost planar, and by applying symmetry, a $TTF^{\bullet+}$ dimer was generated with short S···S (3.417 and 3.271 Å) and C···C (3.323 Å) contacts. Each dimer is surrounded by six $Co(pdms)_2$ molecules and interacts with them through several short contacts and weak hydrogen bonds (Table S2), forming a zig-zag structure along the [101] direction with the $Co(pdms)_2$ molecules at the corner and the $TTF^{\bullet+}$ dimer as segment (Figure 1a). The zig-zag chains interact with each other in the $(10\bar{1})$ plane through hydrogen bonds and O2···S3 (2.953 Å) and O2···C9 (2.887 Å) short contacts to form a 2D sheet. Finally, the sheets interact with each other through various O···S, S···C and O···C short contacts to give a fully interacting 3D structure (Figure 1b).

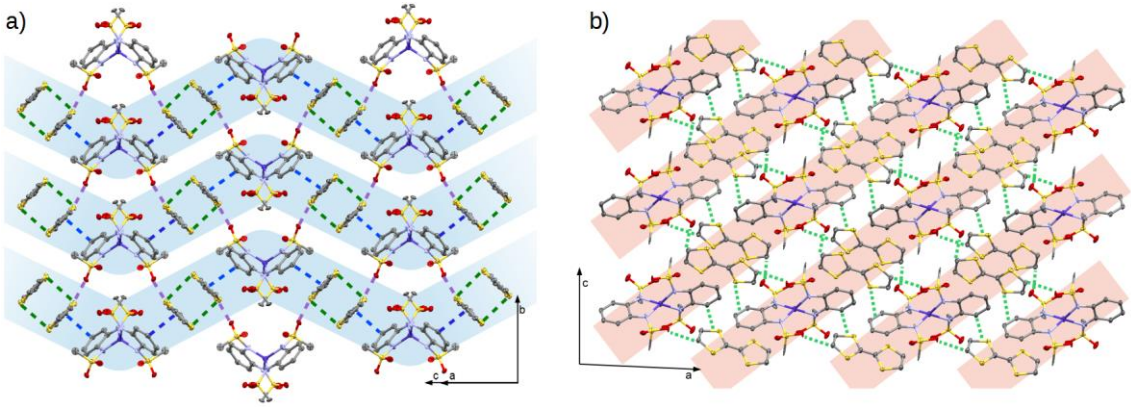

Figure 1. a) Crystal packing in the $(10\bar{1})$ plane. Blue wave represents the zig-zag chains, the dashed lines indicate the short contacts between molecules (green for S···S, blue for C···C, purple for S···O); b) crystal packing in the (010) plane. The pink rectangles represent the 2D sheets, and the dashed lines indicate the short contacts between molecules.

Physical properties. Cyclic voltammetry was performed using an Ag/Ag^+ reference electrode (Figure 2a). Compounds used for the electrochemical experiments, **1-Co** and TTF show similar electron donation abilities with the first oxidation potentials of 0.41 V for TTF and 0.43 V for **1-Co**. The first oxidation process of the metal complexes and TTF can take place simultaneously to give radicals $[Co(pdms^{\bullet-})_2]$ and/or $TTF^{\bullet+}$. X-ray absorption near-edge spectroscopy (XANES) was performed at 298 K at the Co K-edge, and both **1-Co** and **2-Co** showed similar spectra. Therefore, only **2-Co** will be discussed (Figure 2b). It is well known that the oxidation state of the metal ion affects the positions of the absorption coefficient peaks in XANES spectra, where the peak shifts approximately 3 eV per unit of oxidation state.[36] From a comparison of the spectra of **2-Co**, $Co^{II}O$, $Co^{II}Co^{III}_2O_4$, and especially the edge position, the oxidation state of the Co ion in **2-Co** is less than +2. The similarity of spectra for both **1-Co** and **2-Co** allow to conclude also on an oxidation state of the Co ion in **1-Co**

lower than +2. Solid-state UV-Vis-NIR spectra of **2-Co** show at least eight absorption bands (Figure S5a-c). The high energy absorptions (> 27500 cm^{-1}) were attributed to the $M(pdms)_2$ unit, and the absorption bands in the range of 27500–8000 cm^{-1} were assigned to the $TTF^{\bullet+}$ molecule.[37] TDDFT calculations were performed in order to clarify the assignment of the lowest energy transition observed. The results of the calculations at the low-energy absorption energies agreed approximately with the experimental data (Figure 2c), allowing for the assignment of the two lowest transition bands. The absorption band at 6000 cm^{-1}, calculated to be at 5863 cm^{-1}, corresponded to transitions from the highest occupied molecular orbital (HOMO) and HOMO–1 (mainly located on the pdms ligand) to the lowest unoccupied molecular orbital (LUMO) (mainly located on $TTF^{\bullet+}$ dimer) (Figure S6). Therefore, this absorption corresponds to a pdms ligand to $TTF^{\bullet+}$ CT. For the second absorption band at 13000 cm^{-1}, calculated to be at 13377 cm^{-1}, the transition was attributed to CT from the cobalt ion (HOMO–5) to the $TTF^{\bullet+}$ molecules (LUMO) and, to a lesser extent, to an intra $TTF^{\bullet+}$ dimer transition (LUMO+1 and LUMO+4).

Infrared (IR) spectroscopy was used to determine the difference in the vibrational bands in these CT compounds.[38] The strong vibrational band observed at 1350 cm^{-1} in the IR spectra (Figure S7a-b) was assigned to the stretching mode of the central C=C double bonds (a_g (ν_3)) of ($TTF^{\bullet+}$). This vibrational mode is normally inactive in the infrared region on the basis of selection rules. However, strong coupling of the $TTF^{\bullet+}$ dimer with the CT transitions promotes this vibration, which corresponds to the out-of-phase coupling of the originally infrared-inactive a_g modes.[39] The splitting of this band was attributed to the unequal charge of the $TTF^{\bullet+}$ molecules inside the dimer.[40]

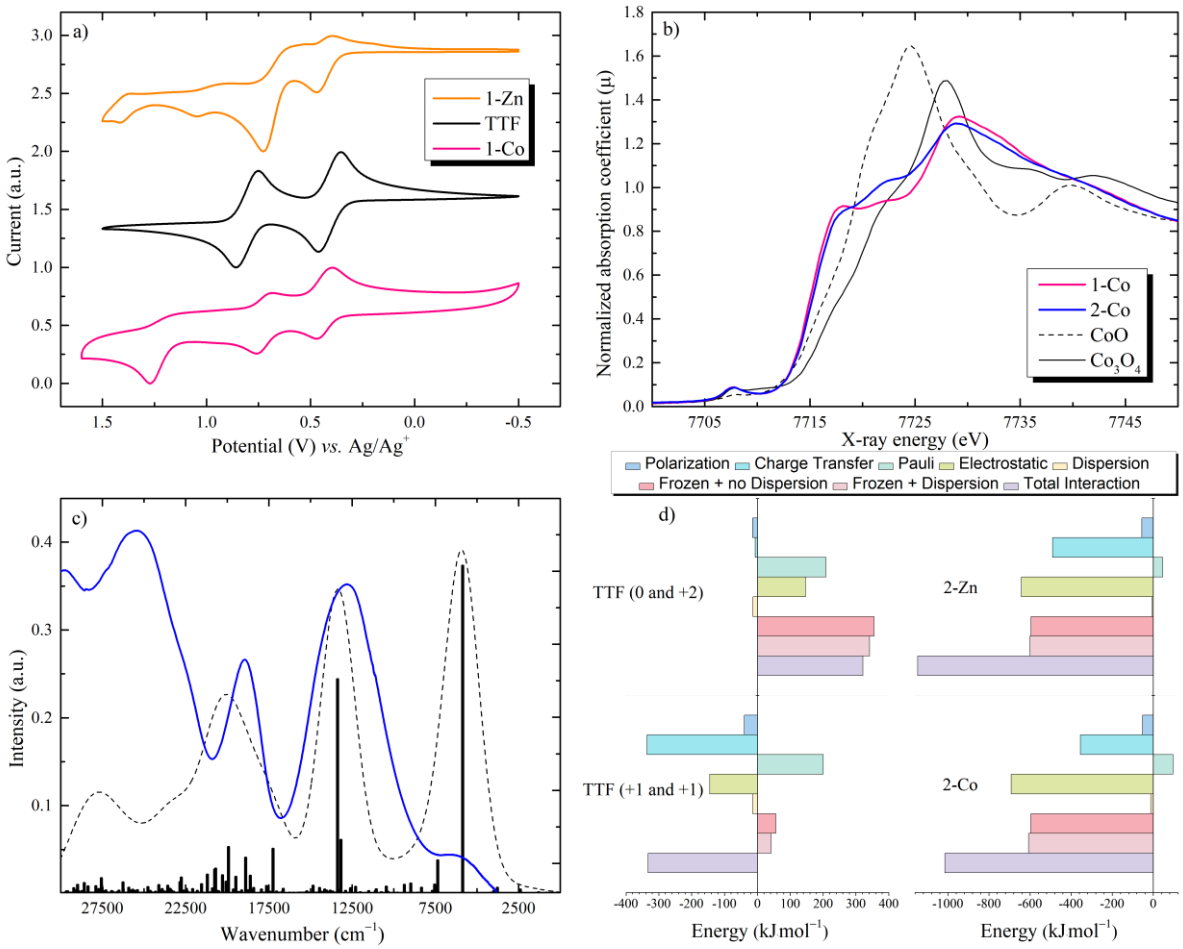

Figure 2. a) Cyclic voltammograms; b) XANES spectra at 300 K. c) The comparison of the UV-vis spectrum of **2-Co** (in blue) and the results of TDDFT calculations (in black). d) The contribution of the different energies to the total energy of the compounds for TTF + TTF^{2+} → $(TTF)_2^{2+}$, TTF^{+} + TTF^{+} → $(TTF)_2^{2+}$ and $(TTF)_2^{2+}$ + $[M(pdms)_2]^{2-}$ → 2-M (M = Zn or Co).

Magnetic properties. The magnetic behaviour of **2-Co**, such as the susceptibility and magnetisation, is in agreement with the previously reported data for **1-Co** (Figure S8, Table S3).[16] Magnetic data for **2-Co** were fitted using PHI software (see discussion section for details)[41] with D = –112 cm^{-1}, $g_{\perp}$ = 2.28 and $g_{\parallel}$ = 2.93 (Figure 3a). **2-Zn** showed a linear evolution of its magnetic susceptibility temperature from 0.012 $cm^3 \cdot K \cdot mol^{-1}$ at 2.5 K to 0.128 $cm^3 \cdot K \cdot mol^{-1}$ at 300 K. In the case of **2-$Co_{0.1}Zn_{0.9}$**, the magnetic behaviour was similar to the magnetic susceptibility temperature of **2-Co** and its room temperature magnetic susceptibility value of 0.345 $cm^3 \cdot K \cdot mol^{-1}$ confirmed that the doping ratio of cobalt ions in the zinc matrix was 10.91%. For **2-Co**, the magnetic hysteresis was observed up to 5 K (Figure 3b) with a coercive field of 350 Oe and a remanent magnetisation of 0.09 μ_B at 2.5 K.

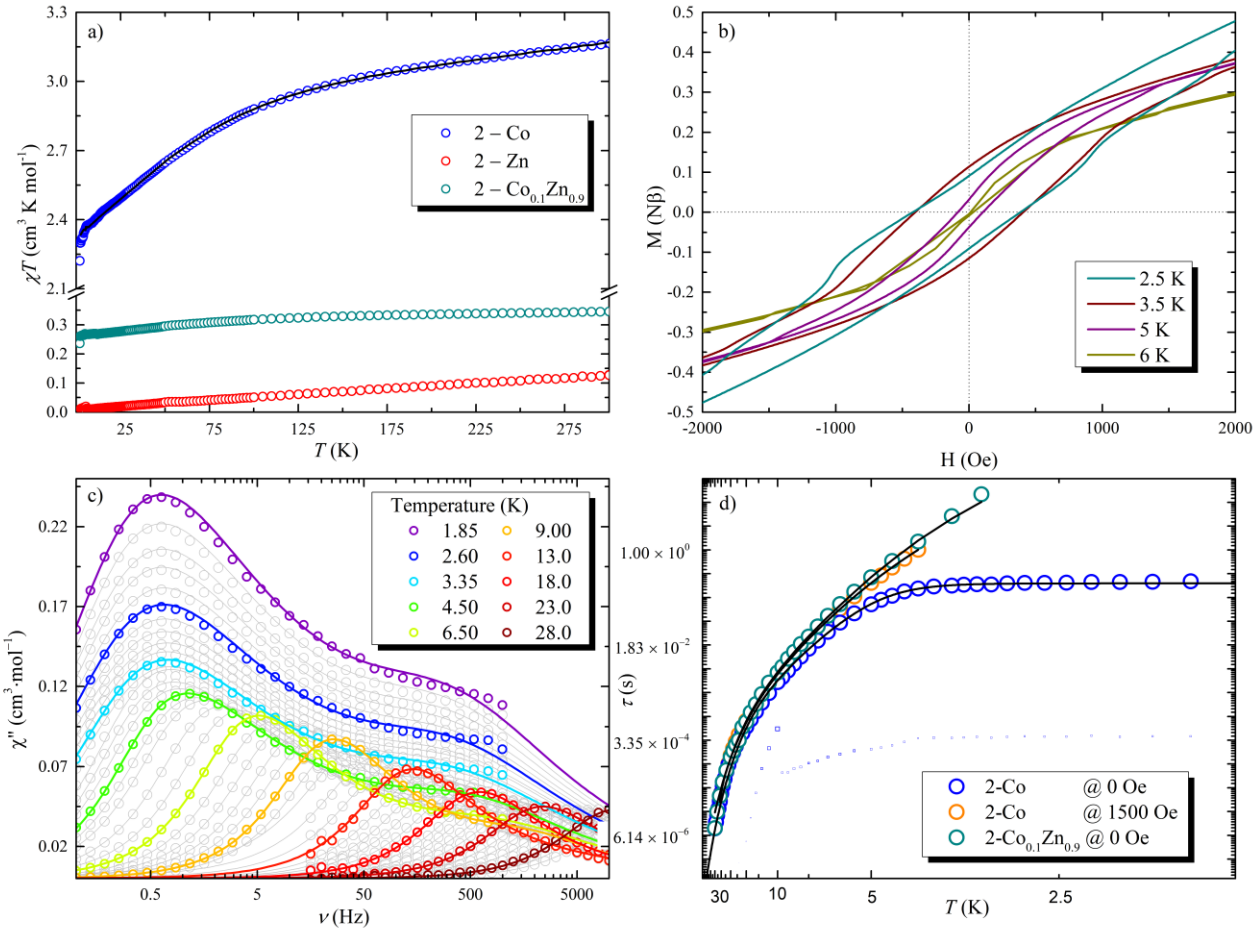

Figure 3. a) Magnetic susceptibility temperature χT as a function of the temperature with open circles representing experimental data. The lines represent the best fit. b) Magnetic hysteresis of the magnetisation of **2-Co** at a sweep rate of 200 Oe·s^{-1} as a function of the temperature. c) The frequency dependence of out-of-phase ac susceptibility (χ'') at 0 Oe in the temperature range of 1.85-28 K. d) The magnetic relaxation time as a function of the temperature. The open symbols represent the experimental data with the symbol size proportional to the contribution of each relaxation (see text). The black lines represent the best fit.

For **2-Co**, the frequency dependence of χ was studied in the range of 0.1–10000 Hz with and without an applied external magnetic field (Figure 3c and Figure S9-S11), and slow relaxation was observed in the temperature range of 1.85–30 K. QTM is dominant below 4.0 K without an external magnetic field. In an optimal field of 1500 Oe, QTM was suppressed. Relaxation times were extracted for all temperatures with or without magnetic fields by using a Havriliak-Negami model (Table S6 and S7).[42] This model is preferred to the usual Cole-Cole model[43] due to the asymmetry of the relaxation process.[44] Without an applied magnetic field, two relaxation times were observed at all temperatures: one was located at higher frequency and with smaller intensity than the main one was located at low frequency (Figure 3c). However, in an applied field, the relaxation process at higher frequency was suppressed (Figure S11). For **2-Co$_{0.1}$Zn$_{0.9}$**, from the frequency dependence in the range of 0.1–1000 Hz without an external magnetic field (Figure S12 and Table S8), the slow relaxation of the magnetisation was observed up to 25 K without QTM and with single relaxation times. In all

cases, a combination of Raman, and Orbach or QTM processes could be used to reproduce the experimental data (see discussion section for detail).

Charge transport properties and magnetoresistance effects: The electrical conductivity measurements were performed on compressed powder-based pellets using a standard four probe technique (Figure 4a). **2-Co** and **2-Zn** showed similar semiconducting behaviours with room temperature conductivities of 2.31×10^{-3} S·cm^{-1} and 1.41×10^{-3} S·cm^{-1} which slowly decreased to be 8.28×10^{-4} S·cm^{-1} and 6.65×10^{-4} S·cm^{-1} at 2 K, respectively. The activation energy of both complexes was not constant over the entire temperature range. The magnetoresistance (MR) effect of the pellet sample of **2-Co** was measured 2 K and 10 K. At 9 T, the resistance increased 4.6% at 2 K and 2.6% at 10 K in comparison to the resistance without an applied magnetic field. (inset of Figure 4a and Figure S13). On the other hand, **2-Zn** showed a negative MR of –0.5% in a magnetic field of 5 T and –0.28% in a field of 9 T.

Theoretical calculations: To determine the oxidation states of the transition metal ions in the complexes, theoretical calculations were performed. Bearing in mind the strong dependence of the choice of the basis set on the methods, such as Mulliken population analysis, Mayer bonding analysis, etc., we employed the more reliable and efficient LOBA method which has been used to accurately predict both the oxidation state and bonding in certain transition metal complexes.[30] The LOBA method was completed by using EDA analysis to quantify the degree of covalency, CT and the contributions of forward and back-donation of synergic bonding in metal complexes.[45] To ascertain the charge distribution, the various interaction energies were computed by using first principles electronic structure methods. The decomposition of the total molecular binding energy into physically meaningful components, such as the frozen density component, dispersion, electrostatic, polarisation, and CT terms, provided us an insight into the charge configuration of the complexes.

The total interaction energy for the $[M(pdms)_2]^{n-}$ fragment in **2-Zn** is more negative than **2-Co**, indicating a larger stabilisation of the ground state (Figure 2d). This stabilisation is mainly due to the larger CT energy for **2-Zn** (–490.5 kJ·mol^{-1}) than that for **2-Co** (–355.0 kJ·mol^{-1}), implying an energetically favourable CT in **2-Co** than that in **2-Zn**. The negligible Pauli energies for both complexes, in comparison to their corresponding frozen energies, indicate that electrostatic interactions are dominate. In more detail, inside the $[M(pdms)_2]^{n-}$ unit, the electrostatic energy shows an appreciable ionic character, whereas for the $TTF^{\bullet+}$ dimer, non-electrostatic interactions between the $TTF^{\bullet+}$ units in the dimer are dominant. The $[M(pdms)_2]^{n-}$ unit is well stabilised with very large negative interaction energies. Introduction of the $TTF^{\bullet+}$ dimer causes an increase in the interaction energies due to the population of the antibonding molecular orbitals, leading to a decrease in the stabilisation of the neutral complexes as compared to the anions. For this reason, CT is important for stabilising the neutral compounds. A CT from the $Co(pdms)_2$ unit to the $TTF^{\bullet+}$ dimer was calculated from the EDA to be 0.73 electrons. Moreover, a second CT of 0.76 electrons occurs from the pdms

ligands to the Co ion (Figure 4c), yielding the mixed-valence states in **2-Co** with the chemical formula $(TTF^{0.56+})(TTF^{0.71+})[Co^{1.24+}(pdms^{1.25-})_2]$.

Band structure and DOS calculations on **2-Co** (Figure 4d, 4e) indicated that the valence and conduction bands merged, which is strong evidence for a metallic state. The large electron density from the Co ion and N and C atoms in the valence bands were attributed to the $[Co(pdms)_2]$ unit, whereas the large electron density from the S and C atoms in the conduction bands were attributed to $TTF^{\bullet+}$. In other words, $[Co(pdms)_2]$ acts as an electron donor, and $TTF^{\bullet+}$ acts as an electron acceptor, which is unusual. In **2-Co**, the pdms ligand is strong σ and π electron donor as compared to $TTF^{\bullet+}$. The band structure shows gaps in the ΓBAY plane for the up spin and in the ZDEC plane for the down spin with minimum values of 817 cm^{-1} and 576 cm^{-1}, respectively. The two planes in the reciprocal space are coplanar with the ac plan in the real space. For **2-Zn**, the valence and conduction bands are completely separated at the Fermi level, similar to a fully gapped organic semiconductor. Like **2-Co**, the large electron density from the N and C atoms in the valence band were attributed to the $[Zn(pdms)_2]$ unit, whereas that from the S and C atoms in the conduction band were attributed to $TTF^{\bullet+}$. (Figure S14).

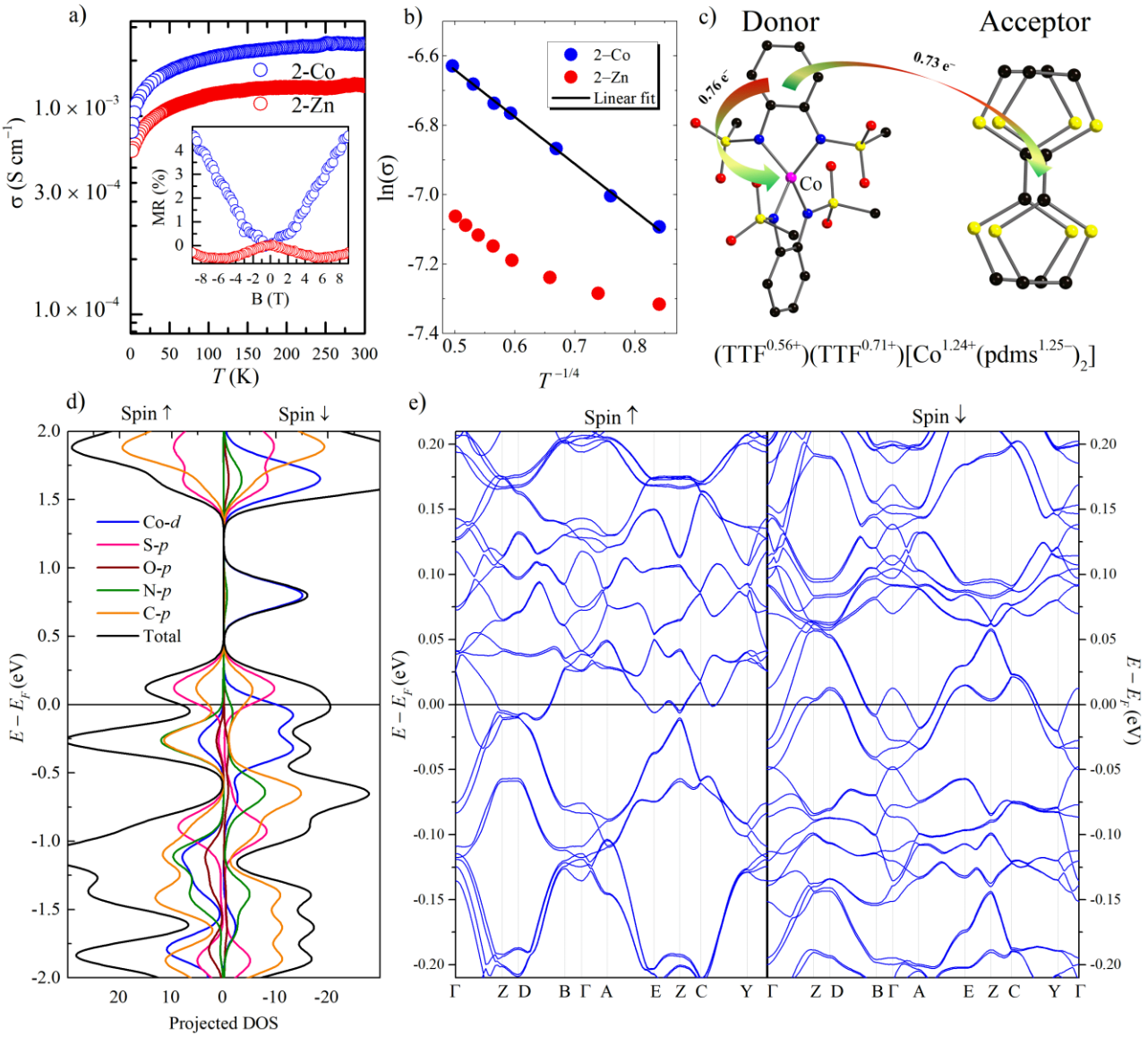

Figure 4. a) Electrical conductivity as a function of the temperature. Insert: the magnetoresistance effect at 2 K as a function of the magnetic field with the magnetic field and the current applied parallel to each other. b) The variable-range hopping conduction in three-dimensional conductivity with p = ¼ in **2-Co** and **2-Zn**. c) Degree of charge transfer and pathway between pdms ligand, Co ion and TTF. d) Projected density of state for **2-Co**; e) Band structure of **2-Co**. High symmetry points in the crystal reciprocal lattice: Γ = (0, 0,0) Z = (0, 0.5, 0) D = (0, 0.5, 0.5) B = (0, 0, 0.5) A = (–0.5, 0, 0.5) E = (–0.5, 0.5, 0.5) C = (–0.5, 0.5, 0) Y = (–0.5, 0, 0).

Discussion

To obtain good electrical conductivity, a partially oxidized molecule with good orbital overlap is necessary.[46] At first glance, **2-Co** and **2-Zn** do not meet this requirement. **2-Co** was obtained by substituting of the two triethylammonium cations in **1-Co** with two $TTF^{\bullet+}$ molecules. The TTF molecules were crystallographically identical, and therefore, the charge of each TTF should be +1 to balance the –2 charge of the $Co(pdms)_2$ unit. The charge of the $TTF^{\bullet+}$ molecules can be calculated by

using the equation $\delta = 4.490 + 10.748(a - b)$,[47] where a corresponds to the central C=C bond length (1.362 Å) and b corresponds to the average C–S bond length between sulphur and central carbon atoms (1.717, 1.718, 1.738, and 1.750 Å). The charge of each $TTF^{\bullet+}$ was determined to be +0.53 on the bases of the structure data. This value is comparable to the theoretical value (+0.56) and corresponds to partially oxidized TTF molecules, compatible with electrical conductivity. On the other hand, the data obtained from XANES showed that the valence state of Co was less than +2. Therefore, it seems there is a diminution of the negative charge of the two pdms ligands to keep the complex neutral.

The theoretical calculations confirmed the above observations. Two CTs from the $Co(pdms)_2$ unit to the TTF dimer, and from the pdms ligand to Co ion occur, meaning that the absolute value of the charge of $TTF^{\bullet+}$ dimer, Co ions and pdms ligands was decreased compared to the initially expected values. Furthermore, a CT from each $TTF^{\bullet+}$ in the dimer with charges of +0.56 and +0.71 remaining occurred. The difference in the charge is confirmed by the splitting of the band at 1350 cm^{-1} in the IR spectra (Figure S7). For **2-Zn**, the charge of the $TTF^{\bullet+}$ was estimated on the bases of the structure data and bond length to be +1.31. This difference in CT was ascribed to the oxidation stability of the zinc ion. Moreover, from the calculations, the charges on the $TTF^{\bullet+}$ in **2-Zn** (+0.87 and +0.97) are larger than those in **2-Co**.

To fit the χT data for **2-Co**, the following procedure was used while ignoring the complexity of the system. First, the contribution of organic radicals was estimated from the data for **2-Zn**. Since the zinc ion is diamagnetic, the magnetisation was attributed to be from the presence of organic radicals. The magnetic susceptibility at room temperature is much smaller than the expected value of 0.5 $cm^3 \cdot K \cdot mol^{-1}$ for a single radical, indicating strong anti-ferromagnetic coupling between radicals. Then, to remove the contribution of the organic radicals in **2-Co**, the signal of **2-Zn** was subtracted before fitting. Finally, although the real charge of the Co ions was estimated to be between +1 and +2, we used +2 in order to be able to compare with previously reported result. No significant changes in the D or g values of **1-Co** and **2-Co** were found. This similarity of magnetic fitting parameters pairs with the comparable XANES spectra for both complexes tends to indicate that CT between Co ion and pdms ligand occur also in **1-Co** with a charge lower than +2 for the Co ion and less than –2 for each pdms ligand.

As mentioned in the Results section, several combinations of relaxation processes can be used to model the magnetic relaxation mechanism for **2-Co** (Table S4). The models differ only by the values of the parameter for the Orbach relaxation process (Table S5). Without an external magnetic field, the models are based on Raman, QTM and Orbach processes with two possible energy barriers: 24 and 152 cm^{-1}. In an applied magnetic field, QTM was suppressed, and Raman and Orbach processes were conserved with energy barriers of 27 and 365 cm^{-1}. However, application of an external magnetic field should only suppress QTM without changing the energy barrier of the system. Therefore the correct model can be determined as a combination of QTM (2.44×10^{-1} s), Raman (n

= 6.59, C = 2.35 × 10^{-5} $s^{-1}K^{-n}$) and Orbach (Δ = 24.1 cm^{-1}, τ_0 = 2.08 × 10^{-4} s) processes without a magnetic field, and Raman (n = 5.53, C = 3.88 × 10^{-4} $s^{-1}K^{-n}$) and Orbach (Δ = 27.0 cm^{-1}, τ_0 = 3.57 × 10^{-4} s) processes with a magnetic field. For **2-Co$_{0.1}$Zn$_{0.9}$**, without a magnetic field, QTM relaxation was not observed in the temperature and frequency ranges studied, and only a single relaxation time, which was determined using Raman (n = 5.83, C = 1.48 × 10^{-4} $s^{-1}K^{-n}$) and Orbach (Δ = 27.3 cm^{-1}, τ_0 = 2.83 × 10^{-4} s) processes, was observed. These results indicate that QTM and the second relaxation time for **2-Co** are due to the dipolar interactions between ions. It should be noted that the parameters are not consistent with the reported ones for **1-Co** complex (Δ = 230 cm^{-1}; τ_0 = 1.1 × 10^{-10} s; n = 3.65; C = 0.088 $s^{-1}K^{-n}$). There are several possible reasons for the differences: The two systems are similar but not identical which would cause small deviations. Δ for **1-Co** was determined by using far IR spectroscopy and used as a restraint to determine the other parameters from the relaxation data. For **1-Co**, the parameters were determined only in the higher temperature region (over 5 K), neglecting the possibility of QTM, and only in bulk without an external field, whereas the parameters for **2-Co** were obtained only from the relaxation time with and without an external magnetic field using a diamagnetically diluted sample.

The electrical conductivity of **2-Co** showed a relatively high value at room temperature and the value varied only by a factor of 3 from 300 to 2.5 K. It is possible that this behaviour can be explained by the semimetallic electronic structure shown in Figure 4e. The Fermi level cuts the conducting bands and valence bands through the high symmetry points, leaving a tiny number of electrons and holes on the Fermi surface. Thus, the overall temperature dependence of the conductivity looks like semimetallic. The electrical conductivity of **2-Zn** showed a lower conductivity, probably related to the full gap structure (Figure S14).

However, because polycrystalline samples are measured, the conductivity should be considered by the variable-range hopping (VRH) theory applicable for the granular materials.[48] The resistance as a function of temperature T is expected as:

$$R_s = R_0 \exp\left(\frac{T_0}{T}\right)^P$$

where R_0 is a constant, T_0 is the characteristic temperature of VRH and p is the hopping exponent. We used p = ¼ for the Mott-type three-dimensional VRH conduction where the density of state is constant near the Fermi level. **2-Co** follows $T^{-1/4}$ temperature dependence of R_s in the temperature range of 2-16 K, however, **2-Zn** shows slight deviation from the $T^{-1/4}$ relation at this temperature region (Figure 4b).[48-49] The difference may be related to the electronic structure or crystal size of the two salts. In spite of the similar temperature dependence of conductivity for **2-Co** and **2-Zn**, the magnetoresistance behaviour is quite different as shown in Figure 4a. The positive MR in **2-Co** could be ascribed to the semimetallic nature of the band dispersion instead of the π-d interaction because of no significant response of MR showing the coupling with the SIM properties. On the other hand, the

negative MR observed in **2-Zn** may be explained by using the quantum interference based on the VRH model.[50]

The multiple CTs process occurred between metal, pdms ligand and TTF due to the strong electron-donating ability of pdms ligand in the large ground energy of $Co(pdms)_2$ anion results in the mixed-valence state in **2-Co**, which has been experimentally characterized by the XANES for the reduction of cobalt ion and IR spectra for the charge disproportionation in TTF dimer, and further confirmed by the theoretical calculations. The relatively high electrical conductivity gives the possibility to make the interaction between magnetic lattice and conducting lattice. The different MR behaviour unveiled the significance of magnetic metal ion in such bifunctional materials.

Conclusions

Electrocrystallization of TTF and magnetic SIM precursor [$Co(pdms)_2$] afforded the first 3D conducting SIM. Theoretical calculations as well as experimental studies clearly showed that there were interactions between localized *d* electrons of the cobalt ion and mobile π electrons of TTF and the pdms ligand. The mixed stacking structure and the close redox potential causes multiple CTs between the components, producing partial oxidation states for the TTF, the Co ion and the pdms ligand, yielding the electrical conductivity to the helium temperature region. Furthermore, based on calculations, [$Co(pdms)_2$] acts as a donor and TTF acts as an acceptor, which is unusual. Meanwhile, **2-Co** is a SIM with opening of the magnetic hysteresis up to 5 K and slow magnetic relaxation up to 30 K. Incorporating high structural dimensionality along with a mixed valence state may be an efficient way to investigate the interactions between the localized physical properties and to induce new physical properties.

ASSOCIATED CONTENT

Supplementary information

Crystallographic data for the structures reported in this article have been deposited at the Cambridge Crystallographic Data Centre, under deposition numbers CCDC 1956269 (Compound **2-Co**) and 1956270 (compound **2-Zn**). Copies of the data can be obtained free of charge via https://www.ccdc.cam.ac.uk/structures/. All other data supporting the findings of this study are available within the Article and its Supplementary Information, or from the corresponding author upon reasonable request.

Corresponding Author

* E-mail: yamasita@agnus.chem.tohoku.ac.jp
shenyongbing17@gmail.com
cosquer.goulven@gmail.com

ORCID

Yongbing Shen: 0000-0002-1277-6071

Goulven Cosquer: 0000-0003-2692-1230

David Chukwuma Izuogu: 0000-0002-1497-2308

Hiroshi Ito: 0000-0001-7029-5869

Alex J. W. Thom: 0000-0002-2417-7869

Takefumi Yoshida: 0000-0003-3479-7890

Shinya Takaishi: 0000-0002-6739-8119

Zhao-Yang Li: 0000-0002-0952-9862

Masahiro Yamashita: 0000-0001-8184-4587

Notes

The authors declare no competing financial interest.

† **Present Address**

Goulven Cosquer: Research Group of Solid Material Chemistry, Graduate School of Science, Hiroshima University 1-3-1 Kagamiyama, Higashihiroshima, Hiroshima, 739-8526, Japan.

ACKNOWLEDGMENTS

This work was partially supported by CREST, JST Grant number JPMJCR12L3. Prof. Masahiro Yamashita thanks the support by the 111 project (B18030) from China. This work was performed under the approval of the Photon Factory Program Advisory Committee (Proposal No. 2018G083, beamline NW2A.

REFERENCES

[1] a) E. Coronado, J. R. Galan-Mascaros, C. J. Gomez-Garcia, V. Laukhin, *Nature* **2000**, *408*, 447-449; b) R. H. Dong, Z. T. Zhang, D. C. Tranca, S. Q. Zhou, M. C. Wang, P. Adler, Z. Q. Liao, F. Liu, Y. Sun, W. J. Shi, Z. Zhang, E. Zschech, S. C. B. Mannsfeld, C. Felser, X. L. Feng, *Nat. Comm.* **2018**, *9*; c) Y. Misaki, H. Fujiwara, T. Maruyama, M. Taniguchi, T. Yamabe, M. Takehiko, M. Mori, S. Tanaka, *Chem. Mater.* **1999**, *11*, 2360-2368.

[2] a) P. Batail, *Chem. Rev.* **2004**, *104*, 4887-4890; b) T. Mori, T. Kawamoto, I. Terasaki, *Phys. Rev. B.* **2007**, *75*; c) J. R. Kirtley, J. Mannhart, *Nat. Mater.* **2008**, *7*, 520-521.

[3] a) Y. Eto, A. Kawamoto, N. Matsunaga, K. Nomura, K. Yamamoto, K. Yakushi, *Phys. Rev. B.* **2009**, *80*; b) Y. Tomkiewicz, A. R. Taranko, J. B. Torrance, *Phys. Rev. Lett.* **1976**, *36*, 751-754; c) I. S. Jacobs, J. W. Bray, H. R. Hart, L. V. Interrante, J. S. Kasper, G. D. Watkins, D. E. Prober, J. C. Bonner, *Phys. Rev. B.* **1976**, *14*, 3036-3051.

[4] a) C. Avendano, Z. Y. Zhang, A. Ota, H. H. Zhao, K. R. Dunbar, *Angew. Chem. Int. Ed.* **2011**, *50*, 6543-6547; b) V. Martinez, A. B. Gaspar, M. C. Munoz, R. Ballesteros, N. Ortega-Villar, V. M. Ugalde-Saldivar, R. Moreno-Esparza, J. A. Real, *Eur. J. Inorg. Chem.* **2009**, 303-310; c) C. Schneider, D. Ukaj, R. Koerver, A. A. Talin, G. Kieslich, S. P. Pujari, H. Zuilhof, J. Janek, M. D. Allendorf, R. A. Fischer, *Chem. Sci.* **2018**, *9*, 7405-7412.

[5] E. Coronado, C. Gimenez-Saiz, C. J. Gomez-Garcia, S. C. Capelli, *Angew. Chem. Int. Ed.* **2004**, *43*, 3022-3025.

[6] F. Setifi, L. Ouahab, S. Golhen, Y. Yoshida, G. Saito, *Inorg. Chem.* **2003**, *42*, 1791-1793.

[7] a) R. Sessoli, D. Gatteschi, A. Caneschi, M. A. Novak, *Nature* **1993**, *365*, 141-143; b) D. Gatteschi, R. Sessoli, *Angew. Chem. Int. Ed.* **2003**, *42*, 268-297.

[8] D. N. Woodruff, R. E. P. Winpenny, R. A. Layfield, *Chem. Rev.* **2013**, *113*, 5110-5148.

[9] T. Yamabayashi, M. Atzori, L. Tesi, G. Cosquer, F. Santanni, M. E. Boulon, E. Morra, S. Benci, R. Torre, M. Chiesa, L. Sorace, R. Sessoli, M. Yamashita, *J. Am. Chem. Soc.* **2018**, *140*, 12090-12101.

[10] G. A. Craig, M. Murrie, *Chem. Soc. Rev.* **2015**, *44*, 2135-2147.

[11] a) K. Hymas, A. Soncini, *Phys. Rev. B.* **2019**, *99*; b) L. Bogani, W. Wernsdorfer, *Nat Mater* **2008**, *7*, 179-186; cM. Yamashita, *Abstr. Pap. Am. Chem. S.* **2015**, *249*.

[12] T. Komeda, H. Isshiki, J. Liu, Y. F. Zhang, N. Lorente, K. Katoh, B. K. Breedlove, M. Yamashita, *Nat. Comm.* **2011**, *2*.

[13] M. J. Martinez-Perez, S. Cardona-Serra, C. Schlegel, F. Moro, P. J. Alonso, H. Prima-Garcia, J. M. Clemente-Juan, M. Evangelisti, A. Gaita-Arino, J. Sese, J. van Slageren, E. Coronado, F. Luis, *Phys. Rev. Lett.* **2012**, *108*.

[14] M. Urdampilleta, S. Klyatskaya, J. P. Cleuziou, M. Ruben, W. Wernsdorfer, *Nat. Mater.* **2011**, *10*, 502-506.

[15] G. Cosquer, Y. B. Shen, M. Almeida, M. Yamashita, *Dalton. T.* **2018**, *47*, 7616-7627.

[16] Y. Rechkemmer, F. D. Breitgoff, M. van der Meer, M. Atanasov, M. Hakl, M. Orlita, P. Neugebauer, F. Neese, B. Sarkar, J. van Slageren, *Nat. Comm.* **2016**, *7*.

[17] B. Liu, A. D. Mclean, *J. Chem. Phys.* **1973**, *59*, 4557-4558.

[18] A. Altomare, M. C. Burla, M. Camalli, G. L. Cascarano, C. Giacovazzo, A. Guagliardi, A. G. G. Moliterni, G. Polidori, R. Spagna, *J. Appl. Crystallogr.* **1999**, *32*, 115-119.

[19] G. M. Sheldrick, *Acta. Cryst. A* **2008**, *64*, 112-122.

[20] B. Ravel, M. Newville, *J. Synchrotron Rad.* **2005**, *12*, 537-541.

[21] G. A. Bain, J. F. Berry, *J. Chem. Educ.* **2008**, *85*, 532-536.

[22] G. Bistoni, L. Belpassi, F. Tarantelli, F. Pirani, D. Cappelletti, *J. Phys. Chem. A* **2011**, *115*, 14657-14666.

[23] P. R. Horn, Y. Z. Mao, M. Head-Gordon, *Phys. Chem. Chem. Phys.* **2016**, *18*, 23067-23079.

[24] Y. H. Shao, Z. T. Gan, E. Epifanovsky, A. T. B. Gilbert, M. Wormit, J. Kussmann, A. W. Lange, A. Behn, J. Deng, X. T. Feng, D. Ghosh, M. Goldey, P. R. Horn, L. D. Jacobson, I. Kaliman, R. Z. Khaliullin, T. Kus, A. Landau, J. Liu, E. I. Proynov, Y. M. Rhee, R. M. Richard, M. A. Rohrdanz, R. P. Steele, E. J. Sundstrom, H. L. Woodcock, P. M. Zimmerman, D. Zuev, B. Albrecht, E. Alguire, B. Austin, G. J. O. Beran, Y. A. Bernard, E. Berquist, K. Brandhorst, K. B. Bravaya, S. T. Brown, D. Casanova, C. M. Chang, Y. Q. Chen, S. H. Chien, K. D. Closser, D. L. Crittenden, M. Diedenhofen, R. A. DiStasio, H. Do, A. D. Dutoi, R. G. Edgar, S. Fatehi, L. Fusti-Molnar, A. Ghysels, A. Golubeva-Zadorozhnaya, J. Gomes, M. W. D. Hanson-Heine, P. H. P. Harbach, A. W. Hauser, E. G. Hohenstein, Z. C. Holden, T. C. Jagau, H. J. Ji, B. Kaduk, K. Khistyaev, J. Kim, J. Kim, R. A. King, P. Klunzinger, D. Kosenkov, T. Kowalczyk, C. M. Krauter, K. U. Lao, A. D. Laurent, K. V. Lawler, S. V. Levchenko, C. Y. Lin, F. Liu, E. Livshits, R. C. Lochan, A. Luenser, P. Manohar, S. F. Manzer, S. P. Mao, N. Mardirossian, A. V. Marenich, S. A. Maurer, N. J. Mayhall, E. Neuscamman, C. M. Oana, R. Olivares-Amaya, D. P. O'Neill, J. A. Parkhill, T. M. Perrine, R. Peverati, A. Prociuk, D. R. Rehn, E. Rosta, N. J. Russ, S. M. Sharada, S. Sharma, D. W. Small, A. Sodt, et al., *Mol. Phys.* **2015**, *113*, 184-215.

[25] F. Weigend, R. Ahlrichs, *Phys. Chem. Chem. Phys.* **2005**, *7*, 3297-3305.

[26] a) A. D. Becke, *J. Chem. Phys.* **1993**, *98*, 5648-5652; b) P. J. Stephens, F. J. Devlin, C. F. Chabalowski, M. J. Frisch, *J. Phys. Chem-Us* **1994**, *98*, 11623-11627.

[27] a) J. P. Perdew, K. Burke, M. Ernzerhof, *Phys. Rev. Lett.* **1996**, *77*, 3865-3868; b) Y. K. Zhang, W. T. Yang, *Phys. Rev. Lett.* **1998**, *80*, 890-890.

[28] H. B. Jansen, P. Ros, *Chem. Phys. Lett.* **1969**, *3*, 140-143.

[29] S. F. Boys, F. Bernardi, *Mol. Phys.* **2002**, *100*, 65-73.

[30] A. J. W. Thom, E. J. Sundstrom, M. Head-Gordon, *Phys. Chem. Chem. Phys.* **2009**, *11*, 11297-11304.

[31] a) J. Pipek, P. G. Mezey, *Int. J. Quantum. Chem.* **1988**, 1-13; b) J. Pipek, P. G. Mezey, *J. Chem. Phys.* **1989**, *90*, 4916-4926.

[32] a) P. O. Lowdin, *Phys. Rev.* **1955**, *97*, 1474-1489; b) P. O. Lowdin, *J. Chem. Phys.* **1950**, *18*, 365-375.

[33] F. Neese, *Wires. Comput. Mol. Sci.* **2012**, *2*, 73-78.

[34] P. Giannozzi, S. Baroni, N. Bonini, M. Calandra, R. Car, C. Cavazzoni, D. Ceresoli, G. L. Chiarotti, M. Cococcioni, I. Dabo, A. Dal Corso, S. de Gironcoli, S. Fabris, G. Fratesi, R. Gebauer, U. Gerstmann, C. Gougoussis, A. Kokalj, M. Lazzeri, L. Martin-Samos, N. Marzari, F. Mauri, R. Mazzarello, S. Paolini, A. Pasquarello, L. Paulatto, C. Sbraccia, S. Scandolo, G.

Sclauzero, A. P. Seitsonen, A. Smogunov, P. Umari, R. M. Wentzcovitch, *J. Phys-Condens. Mat.* **2009**, *21*.

[35] Y. Hinuma, G. Pizzi, Y. Kumagai, F. Oba, I. Tanaka, *Comp. Mater. Sci.* **2017**, *128*, 140-184.

[36] B. Yildirim, H. Riesen, *15th International Conference on X-Ray Absorption Fine Structure (Xafs15)* **2013**, *430*.

[37] a) M. Yoshizawa, K. Kumazawa, M. Fujita, *J. Am. Chem. Soc.* **2005**, *127*, 13456-13457; b) R. Bozio, I. Zanon, A. Girlando, C. Pecile, *J. Chem. Phys.* **1979**, *71*, 2282-2293; c) J. B. Torrance, B. A. Scott, B. Welber, F. B. Kaufman, P. E. Seiden, *Phys. Rev. B.* **1979**, *19*, 730-741.

[38] A. R. Siedle, G. A. Candela, T. F. Finnegan, R. P. Vanduyne, T. Cape, G. F. Kokoszka, P. M. Woyciejes, J. A. Hashmall, *Inorg. Chem.* **1981**, *20*, 2635-2640.

[39] C. Bellitto, M. Bonamico, V. Fares, P. Imperatori, S. Patrizio, *J. Chem. Soc. Dalton.* **1989**, 719-727.

[40] M. E. Kozlov, K. I. Pokhodnia, A. A. Yurchenko, *Spectrochim. Acta. A* **1989**, *45*, 437-444.

[41] R. S. Mulliken, *J. Chem. Phys.* **1955**, *23*, 1833-1840.

[42] R. S. Mulliken, *J. Chem. Phys.* **1955**, *23*, 1841-1846.

[43] I. Mayer, *Int. J. Quantum. Chem.* **1986**, *29*, 73-84.

[44] M. A. Natiello, J. A. Medrano, *Chem. Phys. Lett.* **1984**, *110*, 445-446.

[45] R. Z. Khaliullin, E. A. Cobar, R. C. Lochan, A. T. Bell, M. Head-Gordon, *J. Phys. Chem. A* **2007**, *111*, 8753-8765.

[46] J. Ferraris, V. Walatka, Perlstei.Jh, D. O. Cowan, *J. Am. Chem. Soc.* **1973**, *95*, 948-949.

[47] T. C. Umland, S. Allie, T. Kuhlmann, P. Coppens, *J. Phys. Chem-Us.* **1988**, *92*, 6456-6460.

[48] Y. Fukunaga, M. Harada, S. Bandow, S. Iijima, *Appl. Phys. a-Mater.* **2009**, *94*, 5-9.

[49] a) R. P. Sharma, A. K. Shukla, A. K. Kapoor, R. Srivastava, P. C. Mathur, *J. Appl. Phys.* **1985**, *57*, 2026-2029; b) P. Sheng, J. Klafter, *Phys. Rev. B.* **1983**, *27*, 2583-2586.

[50] a) K. D. Bozdag, N. R. Chiou, V. N. Prigodin, A. J. Epstein, *Org. Electron.* **2013**, *14*, 1419-1423; b) V. L. Ngueyn, B. Z. Spivak, B. I. Shklovskii, *Zh. Eksp. Teor. Fiz+*. **1985**, *89*, 1770-1784.